J Mater Sci (2007) 42:3440–3453
DOI 10.1007/s10853-006-1023-6

A gas phase analysis technique applied to in-situ studies of gas–solid interactions

Clara Anghel · Qian Dong

Received: 18 April 2006 / Accepted: 25 September 2006 / Published online: 20 January 2007

Abstract An ultrahigh vacuum technique using mass spectrometry for in-situ investigations of gas–solid interactions is described in this paper. Examples of chemical reactions (oxidation, hydration) between solids and gas mixtures, dissociation of gases on solid surfaces, outgassing of solid materials and permeation of gases through membranes are discussed where the experimental arrangement is explained in detail. This Gas Phase Analysis (GPA) technique can be used at temperatures from room temperature to 1200 °C and at pressures up to 1 atm. Aspects related to sample preparation, isotopic gas mixture selection, data acquisition, calibration and interpretation of the experimental data are also addressed.

Introduction

The history of mass spectrometry begins in the late 19th century, when J.J. Thomson together with his colleagues at Cavendish Laboratory in Cambridge discovered the electrons, analyzing a beam of cathode rays [1]. Thomson found that the beam was made of particles (later called electrons) with well-defined mass, m, and electric charge, z. In this way the ratio m/z could be used to characterize charged particles [1]. Thomson also showed that the electron beam could be diverted by an electric and/or a magnetic field [1]. In mass spectrometry, the ions, which are produced in the ion source, are separated according to their m/z ratio. After being separated, ions with specific m/z are directed towards the detector region of the mass spectrometer. After Thomson's discovery, progressive development of the ionization methods, analyzers, detectors as well as computer-automation and implementation of libraries with mass spectra made mass spectrometry a reliable, inexpensive and easy to use experimental tool. Nowadays, devices like ionchip™ (Microsaic Systems) [2], which is the first quadrupole mass spectrometer chip, and ''electronic nose'' [3] are just a couple of examples of high-tech mass spectrometry applications.

A comprehensive description of the analysis of gas compositions using mass spectrometry is presented by Řepa et al. [4]. In many publications, mass spectrometry has been used as a main analyzing technique to study specific processes: Hultquist et al. [5] have examined the reaction of Fe with ^{18}O-containing water/oxygen gas mixtures at 300 °C; Levchuk et al. [6] have studied deuterium permeation through Eurofer and α-alumina coated Eurofer; Haugsrud [7] investigated the effect of H_2 and H_2O on the high-temperature oxidation of Ti; Sasaki and Yoshida [8] have introduced new insights related to the reaction of photo-oxidized GaAs with Ga.

In this paper, the methodology of using the in-situ Gas Phase Analysis (GPA) technique to study a wide range of gas–solid interactions is described. The following types of investigations are presented with some examples:

– Studies of *gas uptake kinetics* in solids exemplified by the oxidation of pure Fe and a Zr-based alloy in oxygen gas,

C. Anghel (✉) · Q. Dong
Division of Corrosion Science, Department of Materials Science and Engineering, Royal Institute of Technology, Drottning Kristinas väg 51,
100 44 Stockholm, Sweden
e-mail: anghel@kth.se

– *Isotopic exchange studies* exemplified by O_2 dissociation on the surface of a wide range of solid materials,
– *Outgassing studies* exemplified by outgassing of air equilibrated oxide layers on Zircaloy-2, and
– *Permeation of gases through oxide membranes* exemplified by oxygen permeation through a 2 mm thick zirconia membrane.

Experimental procedure

Sample preparation

In the GPA technique the changes in the gas phase are used as a probe of the reaction between a solid and a gas or a gas mixture. A multitude of solid materials can be studied such as metals, alloys, semiconductors, oxides, nitrides and polymers. Approximations to simple sample geometries (plate, tube, sphere) are used for calculation of transport properties such as diffusivity and permeability, by using solutions of appropriate differential equation of diffusion.

Surface preparation

The sample preparation depends on the sample material and the purpose of the experiment. Metallic samples are typically polished down to 2400 mesh SiC paper, rinsed in ethanol and outgassed. If the aim in a subsequent surface analysis is to study the changes of the surface topography due to the interaction with a gas or a gas mixture, the surface finishing is preferably done by using <1 μm diamond paste and then the sample is ultrasonically cleaned in acetone and finally outgassed in the GPA-equipment.

Oxides are usually cleaned by outgassing at high temperatures before the experiments.

In addition to pure metals, alloys, semiconductors or oxides also coated or pre-hydrated samples can be used.

Surface coating

Coating of solid surfaces with porous, highly active catalysts, such as Pt, have been [9–11] done using a sputter coater.

Hydrogen-charging

Hydrogen charging of metallic or oxide samples using the GPA technique has been used to produce samples with known contents of hydrogen (or deuterium) [9, 12, 13].

Gas Phase Analysis (GPA) equipment

The GPA equipment presented in Fig. 1 consists of three main parts:

1. A ''virtually closed'' reaction chamber
2. A gas handling system
3. A mass spectrometer (MS) placed in an ultra high vacuum (UHV) chamber

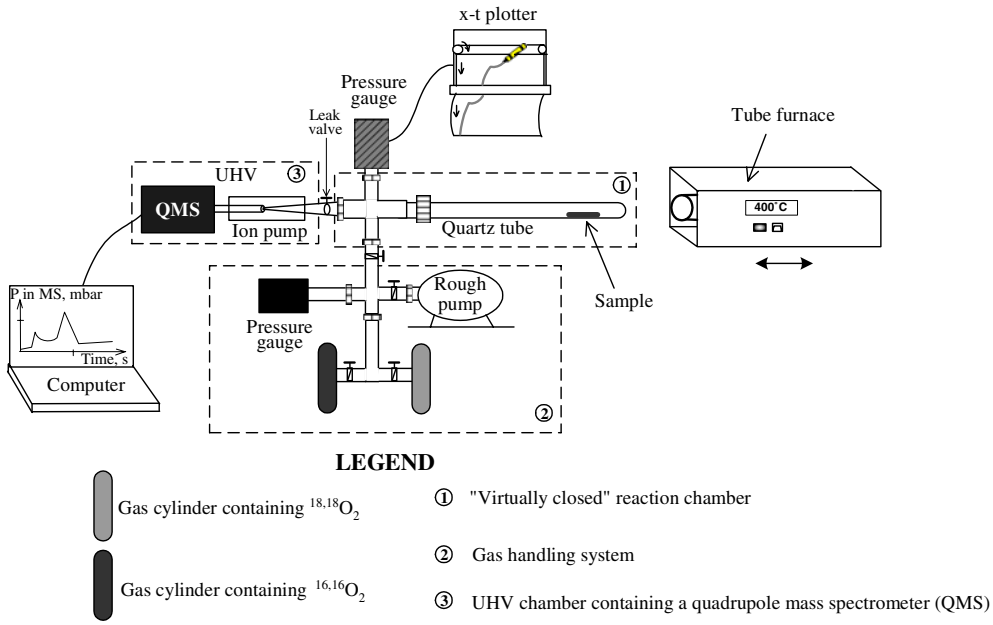

Fig. 1 Schematics of the GPA equipment

These parts are separated by UHV valves.

In Fig. 1, the *''virtually closed'' reaction chamber* consists of a silica tube and a stainless steel (SS) cross. The requirements that need to be fulfilled in the selection of the reaction chamber material include negligible reactivity and gas release during the experiments. The reaction chamber can be heated with a *tube furnace* up to 1200 °C. The *gas handling system* allows inlet of high purity isotopic gas mixtures (two cylinders containing different oxygen isotopes are illustrated in Fig. 1) in the reaction chamber. The total pressure in the reaction chamber is measured using an absolute pressure gauge and can be recorded on an x-t plotter. Pressures up to 1 atm. can be used.

A *mass spectrometer*, placed in an UHV chamber is pumped with an ion pump and used to continuously monitor the gas composition in the reaction chamber via a leak valve. An essential feature is a direct connection, via a glass tube, from the leak valve to the ionisation part in the MS. This arrangement improves the sensitivity and accuracy for the detection of the gases in the reaction chamber. The mass spectrometer is made of the following main parts [14]:

- ionisation source
- mass analyser
- ion detector
- data recording unit

During analysis, the gas is ionised by electron bombardment and the positively charged ions are then directed, using ion optics, to the *quadrupole analyser*, where they are separated according to their mass to charge ratio (m/z). From the analyser, ions with specific m/z (resonant ions) are directed towards the *detector*. Two types of detectors can be used: Faraday Cup and *Electron Multiplier*. The *Faraday Cup* measures the ion current directly and the *Electron Multiplier* magnifies the electric current, which is proportional to the ion flux and gas pressure. The sensitivity of the Faraday Cup is relatively low. Therefore, for pressures lower than approximately $1 * 10^{-10}$ mbar, the electron multiplier is used. From the detector, the signals are transmitted to an electrometer and converted into partial pressures. The resulted mass spectra are displayed on the computer screen. Different types of spectra can be obtained but the most commonly used is the time-based spectrum, which displays the partial pressure of the pre-selected m/z values vs. time.

The setup for the GPA technique can be adapted for different types of measurements: oxidation, hydration, isotopic exchange, outgassing (vacuum annealing), and permeation of gases through membranes. After the introduction of the sample in the reaction chamber, the following steps are common for all these types of measurements:

1. The reaction chamber (with sample) is pumped with a mechanical rough pump for 10 minutes. By this procedure, the pressure in the reaction chamber reaches approximately 10^{-3} mbar.
2. The reaction chamber is then pumped with an ion pump via a glass connector from the leak valve to the MS. The leak valve is fully opened and the pumping is typically done for 12 h at room temperature. By this procedure, more than 50% of the water, which was adsorbed on all surfaces (reaction chamber walls and sample), will desorb [14, 15].
3. The sample and the reaction chamber are cleaned by outgassing at elevated temperatures. The chosen temperature depends on the sample preparation and on the purpose of the experiment. By this procedure, the remaining adsorbed water and the contaminants from sample preparation are removed. Control over the surface coverage of water is essential in many applications. (For example, it was found that adsorbed water could block active sites on solid surfaces for H_2 and CO dissociation [16].)

The next steps depend on the type of the experimental setup in use.

GPA is a useful tool for characterization of complex processes, identification and characterization of reaction mechanisms and transport modes (transport in molecular and/or dissociated form). In-situ information is obtained by combining manometric and mass spectrometric data. A complementary isotopic sensitive technique such as Secondary Ion Mass Spectroscopy (SIMS) can be used to characterize the reaction products [5, 17–20].

The obtained SIMS depth profiles provide useful information such as: oxide growth position [9, 12, 20], identification of the oxide/metal interface [9], hydride formation [21], dominating transport mode [22], identification of oxides with different stoichiometry (different metal/oxygen signal ratio) [23,24].

Principle of GPA analysis

Oxidation, hydration and isotopic exchange studies

In Fig. 1, the standard experimental setup used for oxidation, hydration and isotopic exchange studies is illustrated.

After cleaning the sample and the reaction chamber by outgassing (as described above), the temperature is set to the exposure temperature and the exposure of the sample to a gas or a gas mixture can be carried out. During the exposure, the total gas pressure in the reaction chamber is monitored using an absolute pressure gauge and is recorded by an *x–t* plotter. The gas uptake in the sample is obtained from the pressure decrease in the reaction chamber. To obtain the background (gas uptake by the reaction chamber material), the experiment is repeated in the absence of the sample. After background subtraction, the ''Ideal Gas Law'' is used to calculate the amount of gas taken up by the sample and the amount of gas expressed in mole gas cm^{-2} is:

$$n = \frac{\Delta P}{1013} \cdot V \cdot \frac{1}{RT} \cdot \frac{1}{A} \quad [\text{mole gas cm}^{-2}] \tag{1}$$

where ΔP [mbar] is the pressure decrease in the reaction chamber during the exposure, V[L] the volume of the reaction chamber, R the universal gas constant = 0.08206 [L atm mol^{-1} K^{-1}], T[K] is the absolute temperature, A[cm^{-2}] is the surface area of the sample

The uptake rate [mole gas cm^{-2} s^{-1}] is given by (Eq. 2).

$$\text{Uptake rate} = \frac{n}{\Delta t} \quad [\text{mole cm}^{-2}\text{s}^{-1}] \tag{2}$$

where Δt (s) is the time in which n [mole cm^{-2}] of gas were consumed in the reaction with the sample.

Let's consider a simple case of the oxidation of a metal Me^{IV}.

$$Me + O_2 = MeO_2$$

During the exposure of Me to oxygen gas, an oxide layer (MeO_2) starts to form (stoichiometric oxide formation is assumed, even if this is not exactly the case for very thin oxide layers). Two methods can be used to calculate the degree of oxidation: oxygen gas consumption method (presented above) and the weight gain method. As the name shows, the oxygen gas consumption method takes in consideration the oxygen consumption from the gas phase during the oxidation reaction. With this method, the evolution of the oxide thickness during oxidation can be obtained. A main advantage is related to the cases showing weight loss during oxidation, where the formation of volatile products can be continuously analyzed with the possibility of identification and quantification. Reaction mechanisms could also be investigated using isotopic gas mixtures. The weight gain method takes into account the solid sample's weight change after oxidation. The oxide thickness is calculated only after the oxidation is finished and the sample is weighted (final oxide thickness). For the case of weight loss, no additional information is obtained. It is important to consider the volatile and spalled products which obviously influence the weight gain. Rahtu et al. [25] presented a special experimental setup for in-situ studies of thin film formation by combining Quartz Crystal Microbalance (QCM) and mass spectrometry and thus the weight change as well as the gas composition and pressure can be continuously monitored.

The oxide thickness, L, (Eq. 3) can be calculated considering the amount of oxygen that has been consumed in the reaction with the metal Me, n [mole O_2 cm^{-2}] (obtained from the two methods).

$$L = \frac{n * M_{MeO_2}}{\rho} \quad [\text{cm}] \tag{3}$$

where L [cm] is the oxide thickness, n [mole O_2 cm^{-2}] the amount of oxygen consumed during oxidation (obtained from the weight gain or oxygen gas consumption methods), M_{MeO2} [g $mole^{-1}$] is the molar mass of the oxide, ρ [g cm^{-3}] is the density of the oxide.

When isotopic gas mixtures are used, for example $^{16,16}O_2$, $^{16,18}O_2$, $^{18,18}O_2$, the composition of the gas mixture can be continuously probed with the MS via the leak valve. The gas consumption during probing is negligible. The partial pressure of each component, P_i is obtained. The total pressure change in the reaction chamber (Eq. 4), ΔP, is therefore the sum of the partial pressure change of each component, ΔP_i.

$$\Delta P = \sum_{i=1}^{x} \Delta P_i \quad [\text{mbar}] \tag{4}$$

Exposure of a solid sample to isotopic gas mixtures can be used to study oxidation mechanisms, hydrogen penetration mechanisms, dissociation of gas molecules on the solid surface as well as exchange between the isotopes in the gas phase and the sample.

Investigation of oxidation mechanisms using oxygen isotopes

To study the oxidation mechanism of metals [9, 11], alloys [9, 12, 20] or semiconductors [10], two stage oxidations can be carried out, first in $^{16,16}O_2$ followed

by exposure in $^{18,18}O_2$. After the oxidation performed with the GPA technique, the oxidation products are analysed with other isotope-sensitive techniques such as SIMS [13, 20, 26], secondary neutral mass spectrometry, SNMS [26], or nuclear reaction analysis, NRA [20].

Studies related to the mechanism of oxide growth on some metals (Me) in exposure to H_2O + O_2 gas mixtures have been published earlier, and just to mention a few: Me = Cr: [17], Me = Fe: [5, 19], Me = Cu: [19].

Chevalier et al. [26] have investigated the formation of Cr_2O_3, NiO, ZrO_2 and Al_2O_3 oxide scales at high temperatures using two-stage oxidation. These oxide scales have different growth modes: Cr_2O_3 and NiO scales are growing mainly by outward metal transport, ZrO_2 mainly by inward oxygen transport and Al_2O_3 by mixed inward oxygen -outward cation transport [26]. It is highlighted that complementary techniques such as TEM or SEM could be useful to conclude about the oxide growth mechanism on alloys with complex composition [26]. Recent studies show that the oxide growth mode can be ''manipulated'' by addition of reactive elements (RE) also called oxygen dissociating elements (ODE) and/or hydrogen [9–13, 26, 27]. It is suggested that the main effect of the RE (ODE) is the increased availability of dissociated oxygen due to higher catalytic activity of the RE and thus increased oxygen gradient across an oxide scale, resulting in increased flux through the oxide scale and enhanced oxide growth at the oxide/metal interface.

Isotopic studies of hydrogen effects on the corrosion mechanisms of metals and alloys

G. Hultquist et al. [27] have found both positive and negative effects of hydrogen on the corrosion behaviour of different materials. Deuterium is a commonly used isotope of hydrogen, which behaves similarly with hydrogen although some isotopic effects are expected, due to the difference in atomic weight of D compared to H. The detection limit of mass spectrometers is lower for deuterium due to a higher background of H compared with D.

The diffusion of hydrogen through an oxide scale either inward, towards the metal substrate or outward towards the oxide/gas interface as well as permeation through an preoxidized metallic membrane takes place as a result of thermodynamic equilibration [27]. Ziomek-Moroz et al. [28] have investigated the corrosion of stainless steel in simulated solid oxide fuel cell interconnect environments. The detrimental effect of hydrogen permeation from the inner side of a stainless steel tube (inner side environment: 3% water vapour + hydrogen) to the outer side of the tube, which was exposed to a virtually hydrogen free environment (air) at 907 K for 96 h have been shown [28]. After exposure, the oxide surface on the airside showed significant differences in the oxide morphology in comparison with a tube exposed to air on both sides with the same conditions of temperature and exposure time. The hydrogen permeation through the stainless steel tube wall caused the formation of flaky oxide layers at the airside in contrast to a uniform scale formed on the air/air-exposed tube [28].

Hydrogen present in oxide scales can generate a modification of the defect concentration and, depending on the hydrogen content, an additional number of metal cation vacancies can be induced [29]. The transport of hydrogen in oxides is a complex process, which is still not very well understood and further case-specific studies are required.

Dissociation of gas molecules on solid surfaces

E. Hörnlund [30] has presented a comprehensive description of the dissociation of diatomic molecules on solid surfaces using GPA and isotopic gas mixtures. Selection of the isotopic gas mixture is essential for the quantification of the dissociation rates. For example, to study hydrogen dissociation on solid surfaces, an isotopic gas mixture of approximately 50% H_2 + 50% D_2 is preferably used (this 1:1 ratio of H to D gives better accuracy in the calculation of the dissociation rate) [30]. The time evolution of the gas composition is measured. The parameter used to evaluate the dissociation rate is the formation rate of the mixed molecules HD. This involves dissociation of the gas molecules on the solid surface and re-association of the dissociated species (combinatorial analysis is used to calculate the statistical equilibrated gas composition) [30].

Isotopic exchange between the molecules from the gas phase and the atoms in the lattice

T. Åkermark [31] has presented a study of oxygen isotopic exchange on solid surfaces. In this type of investigations, one isotope is present in the gas phase and another isotope of the same element is present in the examined sample. For example, to study oxygen exchange in zirconia, exposures of $Zr^{16}O_2$, as starting material, to $^{18,18}O_2$ gas can be used. The formation of the mixed molecules $^{16,18}O_2$ in the gas phase is then a result of the exchange between oxygen from the gas

phase and oxygen from the zirconia lattice. SIMS can further be used to analyse the depth distribution of the oxygen isotopes and to evaluate the transport mode (volume and/or interface diffusion) [32] and the diffusion parameters of oxygen isotopes in the oxide [22].

During the calculation of the isotopic gas mixture composition, the following parameters must be considered:

- the natural abundance of stable isotopes
- fragmentation of the molecules in the MS due to the electron ionization
- sensitivity factors.

These parameters are discussed in a forthcoming section.

Outgassing studies

In Fig. 2, a setup for outgassing studies is presented. The aim of the outgassing experiment is to quantify the amount of gas released during the exposure of a solid sample in vacuum (ex. hydrogen present in a metal or an oxide). Low gas release from the reaction chamber is required. In comparison with the setup shown in Fig. 1, in Fig. 2 the silica tube was removed, and the sample is introduced directly inside the SS chamber. A limitation of this setup is the sample size, due to the size of the SS cross. The setup from Fig. 1 can also be used for outgassing at higher temperatures than 100 °C as well as with more complex sample geometries.

The gas flux vs. time in outgassing of a sample with a specific geometry and the appropriate solution of the differential equation of diffusion can be used to estimate the diffusivity and initial gas content. The

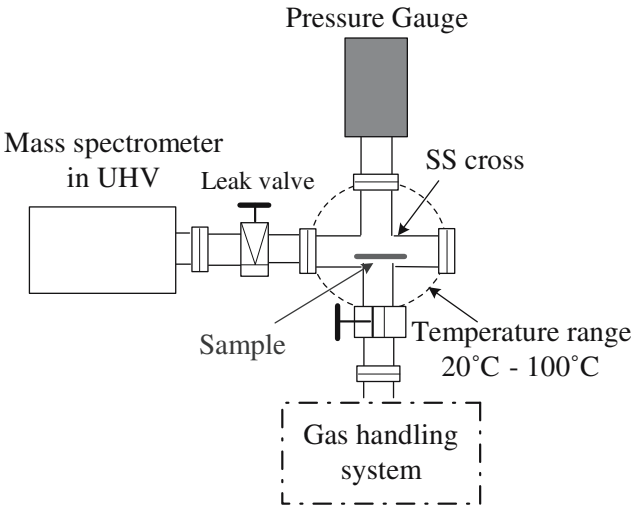

Fig. 2 Setup for outgassing experiments at low temperatures

solution for a plate-like geometry (Eq. 5) for outgassing of an oxide scale of thickness "L" is shown in Fig. 3.

The calculation is based on the following boundary conditions:

a. the initial concentration of gas in the oxide scale is uniform and is equal to C_1.
b. No gas flow from the oxide scale into the metal substrate takes place

The effective diffusivity of the gas and the initial gas concentration in the oxide scale can be evaluated. The effective pore diameter of oxides can also be estimated. A more detailed description of the model used to characterize the release of gas from samples with different geometries can be found elsewhere [33, 34].

A study devoted to quantitative outgassing of water and hydrogen from different materials has been presented by Åkermark et al. [35].

Permeation studies

The setup used for permeation studies, shown in Fig. 4, consists of an outer silica tube, an internal membrane tube and two mass spectrometers, each equipped with a quadrupole analyser. The gas composition is simultaneously analysed at the low-pressure (LP) side and at the high-pressure (HP) side of the membrane. The pressure of the gas is maintained constant at the HP side during the exposure, and the gas composition is probed with the MS via a leak valve (negligible consumption by probing). At the low-pressure side, the leak valve is fully opened to the MS and the permeated gas flux is measured continuously.

The first step is the cleaning of the tubes by outgassing. Then, the permeation experiment can start, by introducing a gas in the HP side. Assuming that the initial concentration (concentration after outgassing) of the diffusing specie is uniform and approximately equal with C_0, after exposure to the gas, the time evolution of the permeated gas flux at the low-pressure

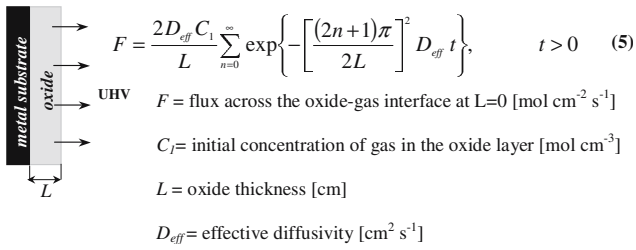

$$F = \frac{2D_{eff}C_1}{L}\sum_{n=0}^{\infty}\exp\left\{-\left[\frac{(2n+1)\pi}{2L}\right]^2 D_{eff}\,t\right\}, \qquad t>0 \qquad (5)$$

F = flux across the oxide-gas interface at L=0 [mol cm^{-2} s^{-1}]

C_1= initial concentration of gas in the oxide layer [mol cm^{-3}]

L = oxide thickness [cm]

D_{eff}= effective diffusivity [cm^2 s^{-1}]

Fig. 3 Mathematical model for outgassing of an oxide scale with thickness L. The solution of the differential equation of diffusion for plate geometry (Eq. 5) describes how the flux of the released gas varies in time in terms of diffusivity, D, and initial gas concentration, C_1

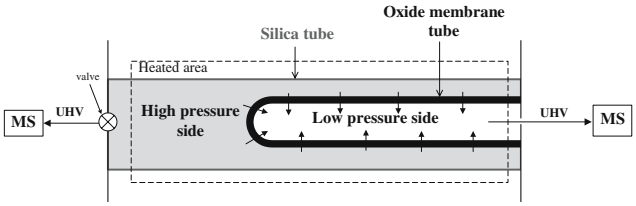

Fig. 4 Reaction chamber setup for permeation experiments

side of the membrane is measured with the MS (Fig. 5).

This curve has the following characteristics:

- at time t = t_0, the gas is introduced at HP side of the membrane and at LP side the pressure of the permeated gas is at background level.
- the time $t = t_c$, so called ''critical'' time, is obtained where the slope for $\frac{dP}{dt} = ct.$ intersects the time axis. (P is the pressure in the MS and t is the time). This so called time-lag method [36, 37], can be used to calculate the diffusivity of a gas, D [$cm^2\ s^{-1}$], through a membrane with known thickness, L [cm]. Equation (6) [36, 37] can be used to calculate the diffusivity of the gas when the surface reactions are not rate limiting.

$$D = \frac{L^2}{6\ t_c} \tag{6}$$

- at time $t \to \infty$ the steady state flux through the membrane is established (no more changes in the pressure at the LP side).

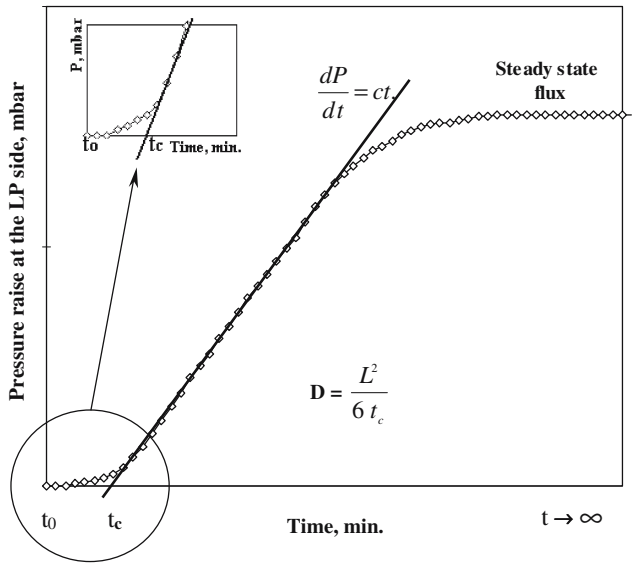

Fig. 5 Time-lag method [36, 37] to evaluate the diffusivity of a gas through a membrane with thickness L

With this setup, permeation of gases such as oxygen, nitrogen, hydrogen [38], He and Ar through oxide membranes (zirconia, alumina or silica) have been tested and our results will be published soon. The gas flux through the membrane is measured and using calibration, quantitative results can be obtained.

MS calibration

To obtain quantitative information, calibration of the MS must be performed regularly [15]. Linear response between the ion signal from the MS and the partial pressure in the reaction chamber is crucial. It is also important to take in consideration the detection limit of the MS for different gases, which depends on the pump rate and background levels (in the UHV and reaction chamber). After subtraction of the background, the MS signals (partial pressures [mbar]) of the examined gases, obtained after background subtraction, are converted in flux unit [μmol gas $cm^{-2}\ s^{-1}$] using in-situ calibration of the MS. There are different quantification methods from which two are described below.

A well-defined amount of a pure gas is introduced in the reaction chamber and the leak valve to the MS is opened to a signal level, which is relevant for the respective experiment. The MS signal of the gas and the corresponding pressure decrease in the reaction chamber (recorded with an absolute pressure gauge) are measured vs. time. This procedure is repeated for different openings to the MS. This is exemplified for oxygen gas in Fig. 6.

From Fig. 6, the gas consumption rate, $\left(\frac{\Delta P}{\Delta t}\right)$ is calculated and is related to the corresponding MS ion signal. The consumption rate of oxygen is converted from mbar s^{-1} units into units of mol O s^{-1} using Eq. 1. The calibration curve shown in Fig. 7 can be used to convert the MS signals into fluxes.

Åkermark et al. [35] have presented an example of MS calibration for hydrogen detection and quantification by outgassing of different samples.

For permeation experiments, an additional method can be used for calibration (gas accumulation method). During the permeation experiments, when the steady state flux is reached, the leak valve is closed, and the pressure increase in the LP side due to the permeation is recorded with an absolute pressure gauge, then the flux of gas is calculated using Eqs. 1 and 2, where the volume is the internal volume of the LP side, the surface area is the area of the membrane and the uptake rate (Eq. 2) represents in this case the gas

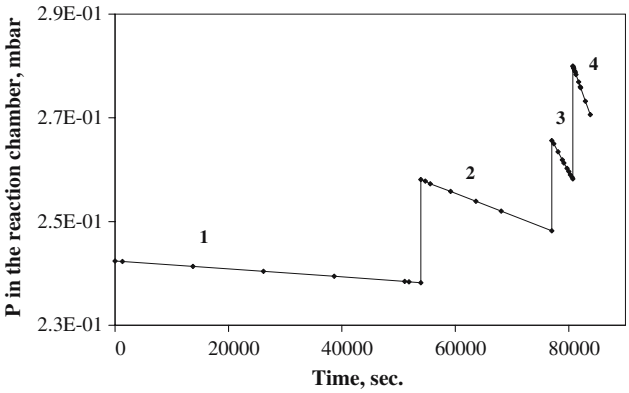

Fig. 6 Oxygen pressure decrease in the reaction chamber for different openings to the MS

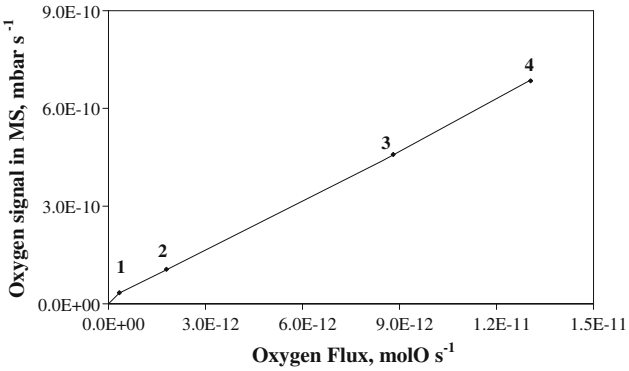

Fig. 7 MS calibration curve. Correlation between oxygen ion signal in MS (using a Faraday Cup detector) and oxygen consumption rate (pressure decrease rate) in the reaction chamber

permeation rate or the flux of the permeated gas. This value is correlated with the steady state signal obtained in the MS.

For investigations of the mechanism of transport (molecular and/or dissociated species) of different gases through membranes, permeation of isotopic gas mixtures through membranes can be performed.

Analytical information

Natural abundances of stable isotopes

In nature all the elements exist in the form of isotopes. All stable isotopes of each element with their abundance are considered when the atomic mass of the respective element is calculated. The natural abundance of a few isotopes as well as their atomic number and weight are summarized in Table 1 [39].

Fragmentation in the MS

In the ionization source, the molecules from the residual gas are ionized by electron bombardment. The most abundant ions are formed by the removal of an electron $X \rightarrow X^+ + e^-$, resulting the so-called molecular ions X^+ ($m/z = M_X$) which represent the base peak. For some molecules, two electrons are also removed during ionization and X^{++} is obtained $\left(m/z = \frac{M_X}{2}\right)$. This forms a minor peak. During ionization, the molecules can also split in smaller parts, forming smaller ions thus generating other minor peaks. The intensity of the minor peaks is normalized relatively to the base peak. The extent of splitting depends on the ionization technique [40]. For example, for electron ionization, the fragmentation pattern of molecules is well defined and depends on the incident electron energy (usually 70 eV).

For our equipment, the fragmentation or cracking pattern of the most commonly used gases is presented in Table 2 [41]. As can be observed in Table 2, three different gases have the base peak corresponding to $m/z = 28$, CO, N_2 and C_2H_4. This means that examining only the base peak is not possible to distinguish between these gases, but considering also the minor peaks, this distinction can be made.

Sensitivity factors

The efficiencies of the ionization process and the transmission of the quadrupole filter are different for different gases and therefore the proportionality between the ion current of a gas and the corresponding partial pressure is dependent on the nature of the gas [41]. The sensitivity of the GPA also depends on the experimental setup. The sensitivity factors for each gas are normalized relative to nitrogen [15]. The procedure to calculate this factor is described in the manual of the equipment [41].

Table 1 Natural abundance, %, of some isotopes as well as their atomic number, Z, and weight [39]

Element	Z	Isotope	Atomic weight, amu	Abundance, %
H	1	^{1}H	1.007	99.985
H	1	^{2}D	2.014	0.0115
H	1	^{3}T	3.016	not stable
O	8	^{16}O	15.9949	99.757
O	8	^{17}O	16.999	0.038
O	8	^{18}O	17.999	0.205
N	7	^{14}N	14.003	99.632
N	7	^{15}N	15.000	0.368

Table 2 Cracking pattern of most common molecules in MS. Minor peaks are presented as relative intensities (base peak intensity = 100) [41]

Molecule	Base peak *m*/z	Minor peaks *m*/*z* Intensity relative to the base peak (100)	
		m/*z*	Relative intensity, %
H_2	2	1	3
O_2	32	16	11
H_2O	18	17	21
H_2O	18	16	1
N_2	28	14	5
N_2	28	29	1
CO	28	12	5
CO	28	16	2
CO	28	29	1
C_2H_4	28	27	64
C_2H_4	28	26	63
C_2H_4	28	25	12

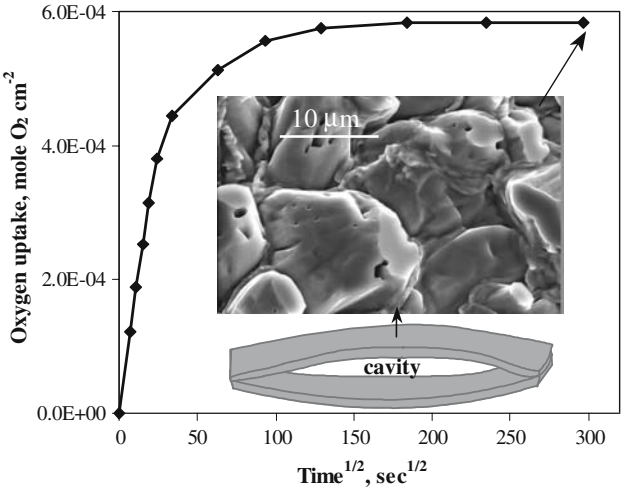

Fig. 8 Oxidation of a pure Fe foil (0.1 mm thick) in approximately 25 mbar O_2 at 900 °C. SEM image of the outer surface of the oxidized Fe foil. A cavity is formed in the center of the oxidized foil due to the outward diffusion of Fe

Examples of studies using the GPA

Oxidation of Fe in O_2 at 900 °C

A 0.1 mm thick iron foil (99.995% metal basis) with the surface area of 1.1 cm^2 was polished with 800 mesh SiC paper, outgassed at temperatures up to 900°C and then exposed to approximately 25 mbar O_2 in 70 cm^3 volume at 900 °C until the whole foil was oxidized. The kinetics of oxygen uptake during oxidation is presented in Fig. 8. An SEM image of the Fe oxide obtained after oxidation is also shown in the figure.

Figure 8 reveals that the oxide is characterized by a multitude of big pores and irregular grains with sizes up to 10 µm. The visual inspection of the oxidized foil showed the presence a well-defined cavity formed in the center of the foil. This cavity is the result of the outward diffusion of Fe during the Fe-foil oxidation and oxide growth at the oxide/gas interfaces. Earlier studies have also shown that Fe-oxide is growing by outward diffusion of Fe [42]. D. Wallinder et al. [43] have studied the influence of hydrogen and Pt-coating on the corrosion of Fe at 500 and 700 °C in oxygen gas. Their main conclusion is that the oxide growth mode can be influenced by the addition of hydrogen and/or a porous Pt-coating. Hydrogen enhanced the outward diffusion of Fe and oxidation at the oxide/gas interface, resulting in increased oxidation rate in comparison with a H-free sample. The porous Pt-coating induced increased oxygen dissociation on the surface with a subsequently increased inward transport of oxygen and oxide growth at the oxide/metal interface (improved scale adherence and lower oxidation rates). The lowest oxidation rate was observed for the hydrogen charged and moderate porous Pt-coated Fe sample [43]. Balanced oxide growth can generate the best oxide quality and therefore lowest oxidation kinetics [12].

Oxidation of Zircaloy–2 in O_2 at 400 and 500 °C

A Zircaloy-2 sample was polished with 2400 mesh SiC paper and cleaned by outgassing at temperatures up to 500°C. The setup presented in Fig. 1 is used for this experiment. The oxidation of the Zircaloy-2 sample was performed in the following steps:

1. Oxidation at 400 °C in 18 mbar $^{16,16}O_2$ for 1 h
2. Oxidation at 400 °C in 349 mbar $^{16,16}O_2$ for approximately 71 h
3. Oxidation at 500 °C in 308 mbar $^{16,16}O_2$ for approximately 28 h
4. Oxidation at 500 °C in 23.6 mbar ^{18}O-containing oxygen gas (approximately 44.5% ^{18}O) for approximately 17 h. The exposure to the isotopic labeled oxygen gas is used to calculate the dissociation rate of oxygen on the preoxidized Zircaloy-2 surface.

Oxygen uptake during oxidation as well as the evolution of the oxide thickness is presented in Fig. 9 (a density of 6 g/cm^3 for the oxide scale was used to calculate the oxide thickness using Eq. 3). The thicknesses obtained by the weight gain and the oxygen gas consumption methods were in good agreement (within 10%). The final oxide thickness of 3 µm was also confirmed by a cross section optical microscopy analysis.

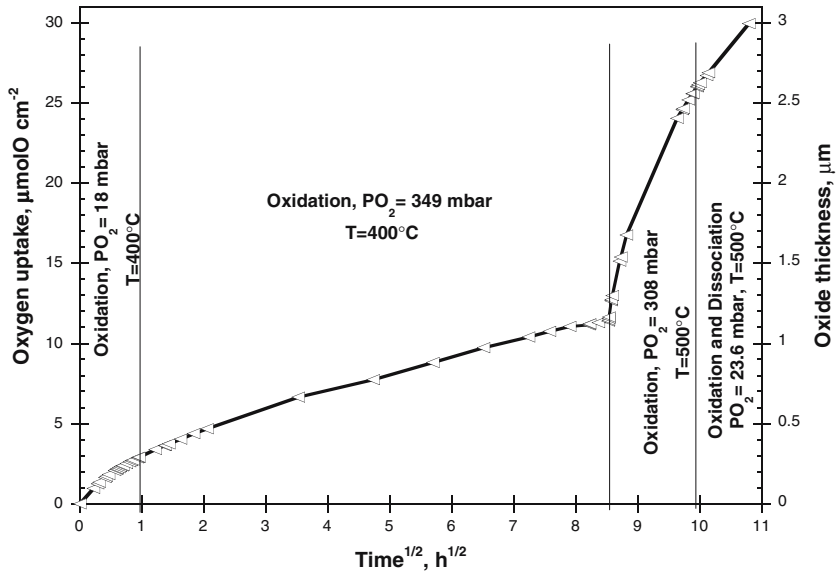

Fig. 9 Time evolution of oxygen uptake and oxide thickness during oxidation of a Zircaloy-2 plate in oxygen gas at 400 and 500 °C. After approximately 100 h of exposure, an isotopic oxygen gas mixture (44.5% ^{18}O) has been used to estimate oxygen dissociation rate at 500 °C

After approximately 100 h of exposure, an isotopic oxygen gas mixture (44.5% ^{18}O) has been used to estimate oxygen dissociation rate at 500 °C. Applying two different oxygen pressures during the oxidation at 400 and 500 °C it can be concluded that a small increase/decrease in the oxidation rate takes place upon pressure increase/decrease for the applied pressure range of 18–349 mbar.

It is known that the oxide grows on Zr-based materials mainly by inward oxygen transport [44]. The mismatch between the oxide and the metal volume (Pilling-Bedworth ratio = 1.56) generates compressive stresses, which can induce formation of defects like pores and microcracks in the oxide during oxidation. The influence of a porous Pt-coating on the oxide growth on zirconium with and without hydrogen charging has been investigated using a combined GPA and SIMS approach [9]. Hydrogen charging had a positive influence on the oxidation of the Pt-coated Zr-sample resulting in a thinner oxide layer. It was found that hydrogen present in the oxide and metal substrate (600 wt ppm D) induced a small but significant Zr outward diffusion generating a beneficial effect on the oxide protection.

As seen in Fig. 9, a 44.5% ^{18}O + 55.5% ^{16}O isotopic gas mixture was used to study oxygen dissociation on preoxidized Zircaloy-2 surface at 500 °C as described further in the paper.

Oxygen dissociation on preoxidized Zircaloy-2 at 500 °C

In the exposure of different materials to oxygen gas, dissociation of oxygen molecules on the surface can take place. The rate of this dissociation reaction defines the catalytic activity of the surface for oxygen dissociation. The formation rate of the mixed oxygen molecules ($^{16,18}O_2$) in the gas phase can be used to calculate the dissociation rate. In the Fig. 10, the formation of $^{16,18}O_2$ during exposure of a preoxidized Zircaloy-2 alloy to approximately 23.6 mbar ^{18}O-containing O_2 gas (44.5 % ^{18}O) at 500 °C is presented. Using the method described by E. Hörnlund [30], a value of approximately 0.03 μmol O cm^{-2} h^{-1} was obtained for oxygen dissociation rate on preoxidized Zircaloy-2 at 500°C. To indicate the importance of this value, the oxidation process has to be considered. The oxide on Zr-based materials is growing mainly at the oxide/metal interface [9, 42], therefore the processes that take place at the O/G interface determine the way in which oxygen is transported trough the oxide layer (O_2 and/or O^{n-}, n=0, 2). The oxidation rate (oxygen

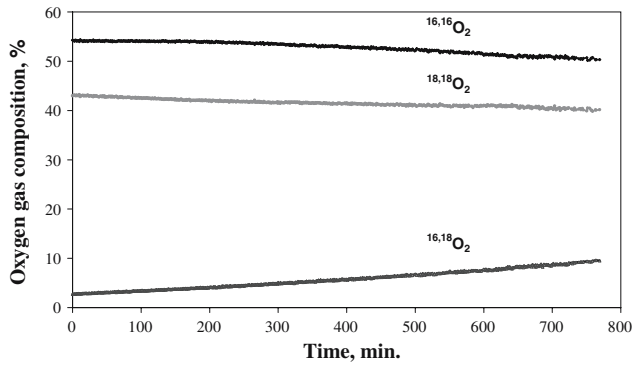

Fig. 10 Oxygen dissociation on preoxidized Zircaloy-2 at 500 °C in approximately 23.6 mbar O_2 (44.5% ^{18}O)

uptake rate) of Zircaloy-2 at 500 °C can be calculated from Fig. 9 presented above using Eq. 2.

At the beginning of the dissociation experiment (after approximately 100 h preoxidation, 2.5 μm oxide thickness), the oxidation rate is approximately 0.3 μmol O cm^{-2} h^{-1} slightly decreasing upon time (parabolic oxide growth). It is important to point out that the oxidation rate is thus 10 times higher than the dissociation rate. This indicates that oxygen transport does not occur only in dissociated form through the oxide scale, other species such as oxygen molecules are also involved in the transport process. This implies that open channels for molecular transport are present in the oxide scale and permit direct access of oxygen molecules to the Zr substrate. Most of the techniques used today for oxidation of metals cannot distinguish the species involved in the transport. The GPA technique can be used also to estimate gas transport parameters such as diffusivity, permeability and solubility in oxide scales when the oxide thickness is known [33, 34].

Outgassing of preoxidized air equilibrated Zircaloy-2 oxide scales at 80 °C

Two Zircaloy-2 samples (with plate geometry) have been used to produce well-defined oxide scales, with known oxide thickness: 1.3 μm and 3 μm. The oxidations were performed in pure O_2 also using the GPA technique. An as-received Zircaloy-2 sample with a naturally formed oxide of approximately 2 nm thickness was also used to obtain the background. All these three samples have been equilibrated in air with low relative humidity at room temperature and then used for the evaluation of the transport properties of the respective oxide scales. The outgassing of water and nitrogen from these three samples at 80 °C using the above-described outgassing procedure is presented in Fig. 11. The term ***F*** is used to express the Flux in μmol cm^{-2} s^{-1} (Eq. 5, Fig. 3) and ***A*** represents the surface area in cm^2.

The outgassing data for the sample with 2 nm oxide thickness was extrapolated for long time outgassing. From Fig. 11, the background outgassing data of the naturally formed oxide scale together with the stainless steel chamber have been subtracted and the resulted fluxes of nitrogen and water for the 1.3 and 3 μm oxide scales were integrated over time (Fig. 12). From this figure, the initial concentration of gases (nitrogen and water), C_1 [μmol cm^{-3}], present in the open pores of these oxide scales can be estimated. Significant amount of molecular species was identified in the Zircaloy-2 oxide scales.

The calculated H_2O and N_2 transport parameters for the two Zr-oxide scales are shown in Table 3. Knowing

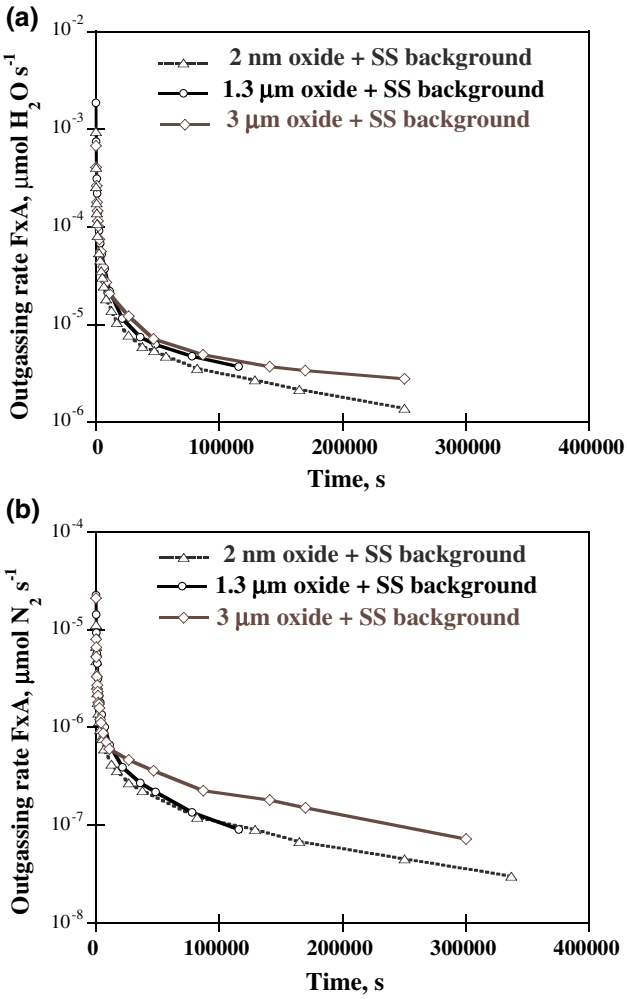

Fig. 11 Outgassing of H_2O and N_2 from three air-equilibrated Zircaloy-2 oxide scales at 80 °C. ***F*** is used to express the Flux in μmol cm^{-2} s^{-1} and ***A*** represents the surface area in cm^2. (**a**) Raw data from outgassing of H_2O from oxidized Zircaloy-2 (**b**) Raw data from outgassing of N_2 from oxidized Zircaloy-2

the initial concentrations of water and nitrogen and the water coverage during the exposure (controlled atmosphere), the effective pore diameter of these oxide scales can be evaluated as described in [33, 34].

Oxygen permeation through an Y-stabilized zirconia (YSZ) membrane at high temperatures

Oxygen permeation through a 2 mm thick YSZ membrane has been measured upon exposure to 1 atm mixed gas (25% O_2, 25%He, 25%N_2, 25%Ar) at temperatures between 400 and 980 °C using the setup presented in Fig. 4 (the permeation of the other gas components is not included in this paper). The steady state flux of oxygen vs. the absolute temperature is shown in Fig. 13. The flux is proportional with $1/L$ (L is

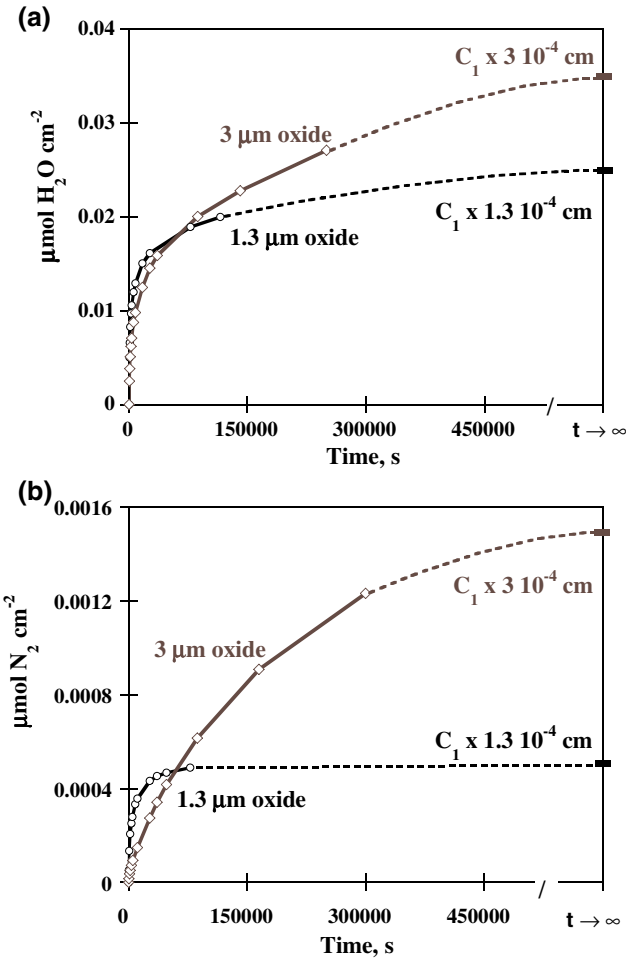

Fig. 12 Integrated Flux over time. C_1 [µmol cm^{-3}] is used to express the initial concentration of gas (nitrogen or water) present in the oxide scale (**a**) Integrated H_2O flux over time for Zircaloy-2 oxide scales (**b**) Integrated N_2 flux over time for Zircaloy-2 oxide scales

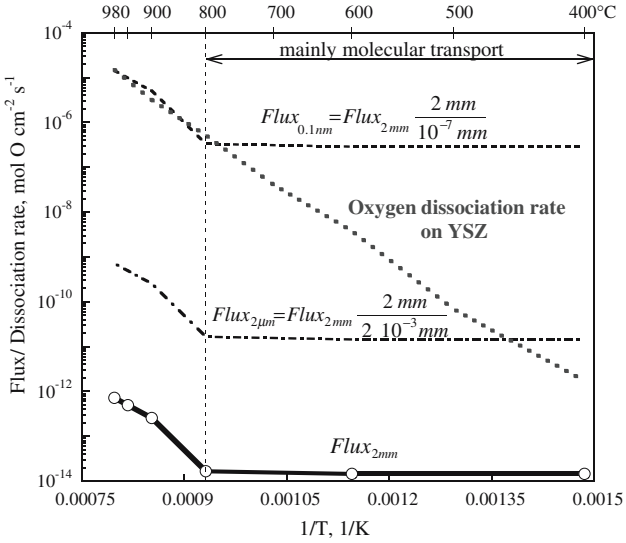

Fig. 13 Oxygen flux through $ZrO_2(Y)$ related to oxygen dissociation rate (P = 250 mbar O_2). Oxygen flux was calculated for thinner oxide membranes (resembling oxide scales) using Eq. 5 (from Fig.3)

the membrane thickness), thus the flux for thinner oxide membranes (resembling oxide scales) have been calculated. Oxide scales can be considered as a special case of membranes, where the metal substrate is the oxygen getter and the oxide grows mainly by inward oxygen transport. Oxygen dissociation rate on YSZ upon exposure to 250 mbar O_2 at the respective temperatures is also presented in the figure (the data are extrapolated from the dissociation rate measured upon exposure to 20 mbar O_2 assuming linear variation with pressure). It can be seen that at temperatures up to 800 °C, the flux is quite low and is not much influenced by the increasing dissociation rate. This is mainly because the transport is divided in three parts: molecular oxygen, oxygen ions and oxygen atoms. The transport pathways for these three species are different and the dissociation rate influences only the transport of dissociated oxygen species. At low temperatures, oxygen is transported mainly in molecular form, so only a significant increase in the dissociation rate can generate increased oxygen flux, or increased oxidation rate, when the oxide represents a scale on a metal substrate [9]. At $T > 800$ °C, oxygen transport is mainly in dissociated form, and for oxide scales thinner than a naturally formed oxide scale, oxygen dissociation rate equals oxygen transport rate (oxygen sticking probability = 1).

Summary of oxygen dissociation data on different materials in 20 mbar O_2

Using the GPA technique, investigations related to oxygen dissociation on various materials have been

Table 3 Transport parameters of H_2O and N_2 in pretransition oxide scales on Zircaloy-2 at 80°C

Sample	H_2O		N_2	
	D_{eff} [cm^2 s^{-1}]	C_1 [µmol cm^{-3}]	D_{eff} [cm^2 s^{-1}]	C_1 [µmol cm^{-3}]
Zircaloy-2 1.3 µm oxide scale	4×10^{-14}	190	2.6×10^{-13}	3.8
Zircaloy-2, 3 µm oxide scales	1×10^{-13}	119	2.1×10^{-13}	5.0

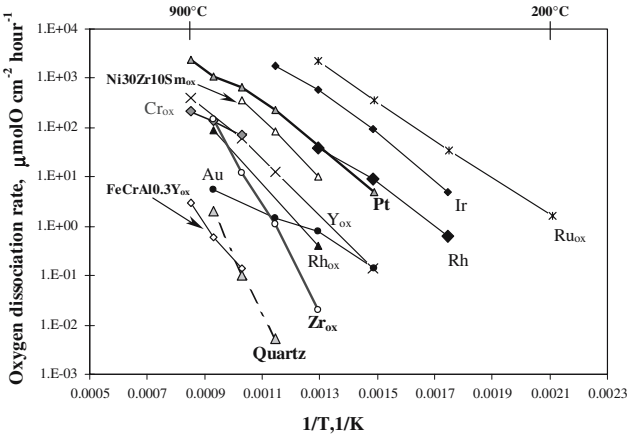

Fig. 14 Oxygen dissociation rate on various materials in 20 mbar O_2 vs. $1/T$

performed [9, 12, 30, 34]. A summary of these experimental results for an oxygen pressure of approximately 20 mbar and temperatures between 200 and 900 °C is presented in Fig. 14. It can be seen that at lower temperatures, the difference between the oxygen dissociation rates on these materials is significant. From the investigated materials, Ru with a naturally formed oxide scale is the best catalyst for oxygen dissociation. Quartz has quite low oxygen dissociation rate, which makes it to be ideal reaction chamber material for this type of measurements because it gives low background.

Conclusions

A straightforward, reliable in-situ method, *Gas Phase Analysis Technique*, using mass spectrometry and labelled gases to study in-situ gas–solid interactions is described with detailed setup configuration and calibration procedures. A summary of studies performed using this technique is also presented. Examples are selected for each type of measurements: oxidation in O_2 gas of Fe and Zircaloy-2, oxygen dissociation on solid surfaces, outgassing of air equilibrated oxide scales (Zr-based oxide scales) and oxygen permeation through oxide membranes (YSZ). By combining GPA with another isotopic sensitive technique like SIMS, the measured compositional changes in the gas phase can be retrieved by analysing the reaction products. Also complementary microstructure analysis techniques will naturally contribute to a better understanding of the information obtained by GPA.

Acknowledgements We wish to thank Doc. G. Hultquist for fruitful discussions during this work. Financial support from Westinghouse Electric Sweden AB and Swedish Foundation for Strategic Research are gratefully acknowledged. Valuable suggestions from John Rundgren, Mike Graham and Peter Szakalos are also appreciated.

References

1. Macoll A (2000) In: Tranter GE, Holmes JL, Lindon JC (eds) Encyclopedia of spectroscopy and spectrometry. Academic Press, p 1241
2. Microsaic Systems, http://www.microsaic.com/ionchip.html, as on 11 April 2006
3. Pavón JLP, Sánchez MN, Pinto CG, Laespada MEF, Cordero BM, Peña AG (2006) TrAC Trend Anal Chem 3:257
4. Řepa P, Tesař J, Gronych T, Peksa L, Wild J (2002) J Mass Spectrom 37:1287
5. Hultquist G, Gråsjö L, Lu Q (1993) Corros Sci 34:1035
6. Levchuk D, Koch F, Maier H, Bolt H (2004) J Nucl Mat 328:103
7. Haugsrud R (2003) In: Proceedings—Electrochemical Society, Vol. 16, High Temperature Corrosion and Materials Chemistry IV, 2003, p 200
8. Sasaki M Yoshida S (1994) J Appl Phys 75:4214
9. Anghel C, Hultquist G, Limbäck M (2005) J Nucl Mat 340:271
10. Hultquist G, Graham MJ, Wee ATS, Liu R, Sproule GI, Dong Q, Anghel C (2006) J Electrochem Soc 153:G182
11. Hultquist G, Hörnlund E, Dong Q (2003) Corr Sci 45:2697
12. Hultquist G, Tveten B, Hörnlund E, Limbäck M, Haugsrud R (2001) Oxid Met 56:313
13. Tveten B, Hultquist G, Norby T (1999) Oxid Met 51:221
14. Niessen WMA (1999) Liquid chromatography-mass spectrometry, Marcel Dekker Inc., New York p. 10
15. Basford JA et al. (1993) J Vac Sci Technol A 11:A22
16. Anghel C, Hörnlund E, Hultquist G, Limbäck M (2004) Appl Surf Sci 233:392
17. Hultquist G, Tveten B, Hörnlund E (2000) Oxid Met 54:1
18. Hultquist G, Mathieu HJ, Gopalakrishnan R, Younes C, Lu Q (1994) Surf Interf Anal 21:800
19. Hultquist G, Gråsjö L, Lu Q, Åkermark T (1994) Corros Sci 36:1459
20. Åkermark T (1998) Oxid Met 50:167
21. Wilhelmsen W, Grande AP (1990) Electroch Acta 35:1913
22. Bassat JM, Petitjean M, Fouletier J, Lalanne C, Caboche G, Mauvy F, Grenier JC (2005) Appl Catal A: General 289:84
23. van Craen MJ, Adams FC (1983) Surf Interf Anal 5:239
24. Plog C, Wiedmann L, Benninghoven A (1977) Surf Sci 67:565
25. Rahtu A, Alaranta T, Ritala M (2001) Langmuir 17:6506
26. Chevalier S, Strehl G, Favergeon J, Desserrey F, Weber S, Heintz O, Borchardt G, Larpin JP (2003) Mat High Temp 20:253
27. Hultquist G, Anghel C, Szakalos P (2006) In: Proceedings of the International Symposium on High-Temperature Oxidation and Corrosion 2005, Nara, Japan, 30th November—2nd December 2005, Mat Sci Forum, 522–523:139
28. Ziomek-Moroz M, Covino BS Jr, Cramer SD, Holcomb GR, Bullard SJ, Singh P Corrosion Nace, Paper No. 04534, 2004
29. Norby T, Widerøe M, Glöckner R, Larring Y (2004) Dalton Trans 19:3012
30. Hörnlund E (2002) Appl Surf Sci 199:195
31. Åkermark T, Hultquist G, Gråsjö L (1996) J Trace Microprobe Tech 14:377

32. Brossmann U, Würschum R, Södervall U, Schaefer H-E (1999) J Appl Phys 85:7646
33. Anghel C, Hultquist G, Dong Q, Rundgren J, Saeki I, Limbäck M (2006) In: Proceedings of the International Symposium on High-Temperature Oxidation and Corrosion 2005, Nara, Japan, 30th November–2nd December 2005, Mat. Sci. Forum, 522–523:93
34. Anghel C (2004) In: Studies of Transport in Oxides on Zr-based Materials, Licentiate Thesis, Royal Institute of Technology, Stockholm, 2004
35. Åkermark T, Hultquist G, Lu Q (1996) J Mater Eng Perform 5:516
36. Shelby JE (1996) Handbook of gas diffusion in solids and melts. ASM International, p.1
37. Barrer RM (1941) In: Rideal EK (ed) Diffusion in and through solids. Cambridge Univ. Press, p. 10
38. Hörnlund E, Hultquist G (2003) J Appl Phys 94:4819
39. CRC Handbook of chemistry and Physics, 85th edn. David R Lide (ed) (2004–2005)
40. Encyclopedia of Spectroscopy and Spectrometry (2000) In: Tranter G, Holmes J, Lindon J (eds) Academic Press
41. MKS book- Operating Manual and Programming Reference, Stanford Research Systems, http://www.thinksrs.com/downloads/PDFs/Manuals/RGAm.pdf, as on 11 April 2006
42. Fehlner FP, Graham MJ (1995) In Marcus P, Oudar J (eds) Corrosion mechanisms in theory and practice, Marcel Dekker Inc., New York
43. Wallinder D, Hörnlund E, Hultquist G (2002) J Electr Soc 149:B393
44. Grandjean A, Serruys Y (1999) J Nucl Mat 273:111